A Drenik et al.

Evolution of nitrogen concentration and ammonia production in N2-seeded H-mode discharges at AUG

Evolution of nitrogen concentration and ammonia production in N_2-seeded H-mode discharges at ASDEX Upgrade

A. Drenik[a, b], L. Laguardia[c], R. McDermott[a], G. Meisl[a], R. Neu[a, d], M. Oberkofler[a], E. Pawelec[e], R. A. Pitts[f], S. Potzel[a], T. Pütterich[a], T. Reichbauer[a, d], V. Rohde[a], M. Seibt[a, d], G. De Temmerman[f], R. Zaplotnik[b], the ASDEX-Upgrade team* and the EUROfusion MST1 team**

[a]*Max-Planck-Institut für Plasmaphysik, 85748 Garching b. München, Germany*
[b]*Jožef Stefan Institute, Jamova 39, SI-1000 Ljubljana, Slovenia*
[c]*CNR, Istituto di Fisica del Plasma ''P. Caldirola'', Milan, Italy*
[d]*Technische Universität München, 85748 Garching b. München, Germany*
[e]*University of Opole, Institute of Physics, Oleska 48, Opole, Poland*
[f]*ITER Organization, Route de Vinon-sur-Verdon, CS 90 046, 13067 St Paul Lez Durance Cedex, France*
See the author list of "A. Kallenbach et al, 2017 Nucl. Fusion 57 102015"
**See the author list "H. Meyer et al 2017 Nucl. Fusion 57 102014"*
aleksander.drenik@ipp.mpg.de

Abstract: Ammonia formation was studied in a series of dedicated nitrogen seeded H-mode discharges at ASDEX Upgrade. The evolution of ammonia formation was investigated with a reference phase before the seeding, and a long, stable flat-top nitrogen-seeded phase. It was monitored with divertor spectroscopy and analysis of the exhaust gas. The amount of the detected ammonia increased continuously over the course of five discharges with the same nitrogen seeding rate. The same trend was observed in the nitrogen density in the core plasma, as measured by charge exchange recombination spectroscopy and other signals, linked to the effects of nitrogen seeding. The results show that the rate of ammonia formation mainly changes with the nitrogen density in the plasma. This density, in turn, was strongly influenced by the nitrogen wall inventory. The spatial distribution of the detected ammonia suggests that a significant contribution to the net ammonia formation is made in plasma-shaded areas, through surface reactions of neutral species.

1. Introduction

In magnetically confined fusion devices, a certain concentration of low-Z impurities is required in the plasma to improve confinement and mitigate the divertor heat loads by promoting radiation in the plasma edge[1]. The latter is an essential feature for ITER where a high fraction of the energy entering the scrape-off layer will have to be dissipated through radiation in order to reduce the divertor heat loads to technologically feasible levels[2]. In fusion devices with carbon-based plasma facing components (PFCs), a sufficiently high concentration of carbon in the plasma was sustained by erosion and migration of the plasma-facing materials[3]. In fusion devices with fully metallic PFCs, such as the full tungsten ASDEX-Upgrade (AUG), JET with the ITER-like wall and most notably, the upcoming ITER, the intrinsic concentration of low-Z impurities is significantly lower, so they have to be introduced into the plasma as seeded gases. Among the tested gases, nitrogen has given the best results both in terms

of confinement enhancement as well as the distribution of radiation in the plasma edge. Thus, under current plans, nitrogen seeding will be a part of the plasma scenarios at ITER.

Besides its beneficial effects on the plasma operation, nitrogen also engages in plasma-surface interaction. It is retained in the plasma-facing surfaces by ion implantation and formation of W_xN and Be_xN[4] which results in a noticeable build-up and legacy of the nitrogen content in the plasma[5,6]. Most importantly, nitrogen seeding has been shown to lead to ammonia production[4,6–8], which could be a potential issue for ITER. Nitrogen seeding in the active phase of ITER operations would lead to formation of partially tritiated ammonia. Retained in the vessel, it would contribute to the in-vessel tritium inventory. More importantly, ammonia would be adsorbed on the active charcoal surface of the ITER cryo pumps. In order to release the tritium-containing ammonia, the cryo panels would have to be heated up to much higher temperatures than originally foreseen, which could significantly reduce ITERs duty cycle. In order to develop reliable estimates of the in-vessel ammonia production at ITER, data from present-day fusion devices are required.

First report of ammonia formation from AUG[7] shows that ammonia is indeed formed during nitrogen seeded discharges and that its subsequent interaction with the in-vessel surfaces results in relatively slow outgassing (compared to other components of the neutral gas) and significant degree of isotope exchange. It also demonstrates that in-vessel produced ammonia can be detected in the neutral gas, pumped from the vessel. Residual gas analysis of discharges with nitrogen seeding at JET shows that formation of ammonia increases with the amount of seeded nitrogen, however large scatter indicates that other parameters could also influence the ammonia formation[6]. In first dedicated ammonia formation experiments at JET[4], it was shown that in a series of discharges with the same or very similar rates of nitrogen seeding, ammonia formation exhibits a significant evolution, increasing continuously both in the timeframe of a single discharge as well as from one discharge to another. In both devices, a significant legacy effect of nitrogen was observed, i.e. detectable levels of nitrogen were detected in non-seeded discharges following the seeded ones, lasting for several (up to 10)[5] discharges before falling back to the intrinsic nitrogen content. The observed nitrogen legacy could impact the observed trends in ammonia formation as well.

In this paper, we present the findings the first dedicated ammonia formation experiment at the full-W AUG, aimed at gaining a deeper insight into the build-up behaviour of the ammonia formation, the underlying processes and the key parameters which drive and define the ammonia formation in a fusion device.

2. Discharge setup and sequence

The experiment was designed as a series of discharges with an identical setup (standard discharge) which would be repeated until the saturation of ammonia formation was observed. The carried out sequence of discharges is listed in Table 1. The discharges were performed on an experimental day with no prior N_2-seeded discharges, so the initial wall inventory was negligible. During the course of the

experiment, the ammonia production was monitored by analysis of the residual gas in the inner divertor (explained in more detail in the following section). The saturation of ammonia formation was observed after five discharges. Following those, three slightly modified discharges were performed.

The standard discharge was designed as a moderately-powered H-mode discharge with I_p/B_T = 0.8 MA/2.5 T, line averaged density of $7 \cdot 10^{19}$ m^{-3}, a long and stable flat-top phase, and a reference phase before the onset of nitrogen seeding. The setup is represented by the time traces of discharge #33032, shown in Fig. 1. The ERCH and NBI heating powers (Fig. 1a) were kept at 1.25 and 7.5 MW respectively and the D_2 fuelling rate (Fig. 1b) was kept at 10^{22} el/s. The N_2 was injected into the private flux region, at the constant seeding rate (Fig. 1b) of $1.2 \cdot 10^{22}$ el/s which was a compromise between a high rate of ammonia formation and keeping the outer divertor in an attached state. The maximum heating power was reached at the time of 1.5 s and lasted until 7.5 s, while the N_2 was seeded between 2.6 and 7.5 s. Thus, the time between 1.5 and 2.6 s is referred to as the reference phase, and the time between 2.6 and 7.5 s is referred to as the flat top phase.
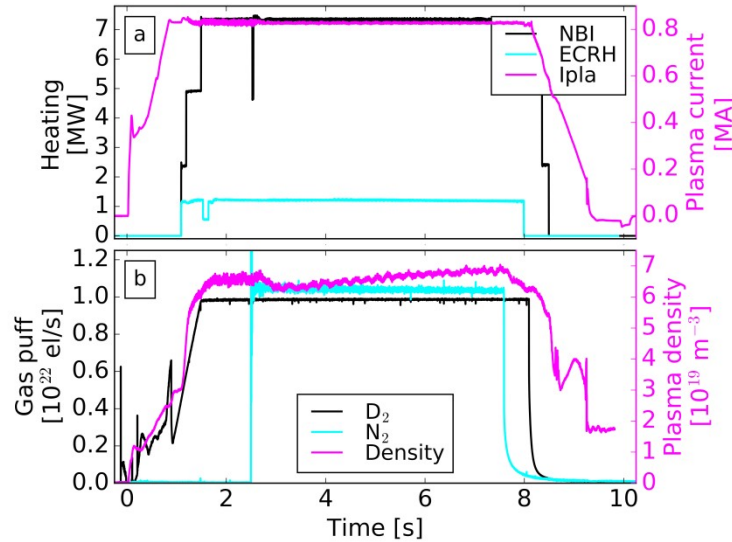
Figure 1:   Discharge setup shown by time traces from discharge #33032, a) auxiliary heating and plasma current, and b) D_2 and N_2 injection rate

After the saturation in the ammonia formation was observed with the inner divertor residual gas analyser, the following variations of the standard discharge were carried out:

- Upward shift: The plasma was shifted upwards by 3 cm with respect to the standard discharge.
- Detached discharge: The NBI heating power was reduced to 5 MW, which resulted in full detachment of the outer divertor at the same seeding rate as in the standard discharge setup.
- Earlier seeding stop: The N_2 seeding was stopped at 5.5 s, 2 seconds earlier than in the standard discharge.

The reference phase of discharge #33028 is considered the non-seeded reference for the experiment, as the walls were contaminated with nitrogen in all of the following discharges. For the requirements of

neutral gas analysis, the last non-seeded discharge prior to the series of eight dedicated discharges is additionally considered, as a reference for the impurity content. The discharge #33032, which was the last one executed with the standard setup, is considered as the representative seeded discharge. The ammonia formation was studied with neutral gas analysis and divertor spectroscopy, which are described in the following sections.

Table 1: List of performed discharges

Discharge in sequence	ASDEX-Upgrade shot number	Remarks	Seeded N_2 [10^{21} atoms]
N/A	33027	Non-seeded reference for residual gas analysis	0
1	33028	N_2 seeding at 57 % of the standard seeding rate	4.6
2 – 4	33029 – 33031	Standard discharge setup	7.8
5	33032	Standard discharge setup (saturation of ammonia production observed in the inner divertor RGA)	
6	33033	Upward shift	7.8
	33034 - 33036	Two failed discharges and a probe test (no plasma in either of them)	0
7	33037	NBI heating reduced to 5 MW with full detachment of the outer divertor	7.8
8	33038	Early stop of N_2 seeding	4.7

3. Neutral gas analysis

a. Neutral gas diagnostic setup

The setup of neutral gas diagnostic system at AUG is shown in Fig. 2. The system features magnetically shielded, differentially pumped residual gas analysers (RGAs) at the inner divertor, the outer divertor, and the midplane, and Baratron absolute pressure gauges. In the outer divertor and the midplane, the low-range pressures (typically below 10^{-4} mbar) are also measured with ionization pressure gauges, however as their response is strongly influenced by the composition of the neutral gas, they are not suited for experiments with impurity seeding. Accordingly, only the data from the absolute pressure gauges are considered in this paper. The divertor pressure gauges are mounted at the same locations as the mass spectrometers, and are calibrated as part of regular maintenance during shut-down periods. The outer divertor neutral gas diagnostic cluster is located in one of the pumping chambers of ASDEX Upgrade. The gas transport from the divertor to the cluster is accordingly governed by the effect of the turbo molecular pump at the end of the chamber, and the in-vessel cryo panel, which is located at the entrance of the pumping chamber. The cryo panel, which is at liquid He temperatures during discharges, is protected with a liquid N_2 shield which prevents it from filling up with impurities with a lower vapour pressure, such as water and ammonia. For D_2, the combined impact of the turbomolecular pump and the cryo panel is evaluated with a D_2 calibration puff at the end of each discharge, and is found to result in a 6-fold reduction of the pressure.
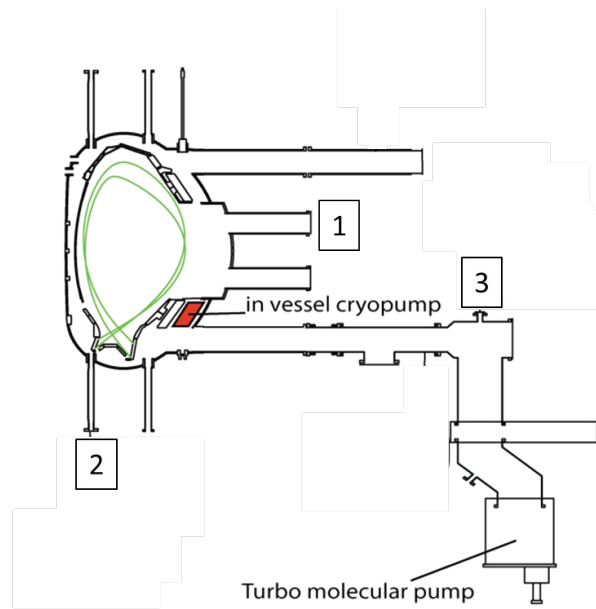
4

Figure 2:   Neutral gas analysis setup at ASDEX-Upgrade. RGAs are located at the midplane (1), in the inner (2) and the outer (3) divertor.

The RGAs used were an MKS HPQ2 (inner divertor), MKS HPQ3 (outer divertor) and a Hiden Analytical HAL 201 RC (midplane). During the discharges, they were set to record the intensity at discrete mass/charge values. The full range of recorded masses varied among the instruments, however it always included the $14 - 20$ AMU/e_0 range (populated by ammonia) and 28 AMU/e_0 (N_2). The scanning times were around 0.5 seconds for the whole mass range. The sensitivity of the mass spectrometers in the divertor, however not in the midplane, measured by injecting N_2 and CD_4 into the AUG vessel, with the divertor cryo pump was warmed up. The cracking patterns of ammonia and methane for all devices were measured in a laboratory vacuum chamber, with the uncertainty of 10 %. The RGA measurements are discussed in the following sub-sections.

b. Nitrogen

As shown in previous analysis at AUG[7] and JET[6], apart from the nitrogen molecule (N_2), there are no other significant contributions to the mass spectra at 28 AMU/e_0. Based on that, the intensity at this mass-charge ratio is attributed solely to nitrogen. The time traces of the partial pressures of N_2 from the RGAs are shown in Fig 3, for the inner (a) and outer (b) divertor, and the midplane (c), in a non-seeded discharge (#33027), and the first (#33028) and fifth seeded discharge (#33032) in the row. Although the two seeded discharges are not directly comparable because of the different seeding rates, time traces from discharge #33028 are relevant as this was the only seeded discharge with only a negligible amount of nitrogen stored in the walls.

In line with previous observations at AUG and JET, the partial pressure of N_2 in the divertor region is strongly dominated by the seeding gas puff, and rises for two orders of magnitude above the

background pressures detected in the non-seeded discharge. In the outer divertor, the wall-stored nitrogen caused an observable increase in the N_2 signal before the seeded phase in discharge #33028. In the outer divertor, the pressure stabilized about 1 s after the start of the seeding, whereas in the inner divertor it continued to slowly increase throughout the discharge. Despite the higher N_2-seeding rate in #33032, the observed N_2 pressure in the inner divertor is not notably higher than in #33028. This is related to the collapse of the high field high density region and discussed in the following sections. The N_2 pressure in the non-seeded discharge in the inner divertor dropped significantly after the discharge phase. This sudden decline is attributed to a change in the gas transport, brought on by the collapse of the pressure gradient, and could impact the transport of other species as well.

In contrast to the divertor, the impact of the gas puff in the midplane is significantly smaller. Please note that the divertor plots are shown in logarithmic scale while the midplane plot is shown in the linear scale. During the discharge phase, the N_2 pressure in the midplane showed only a hardly noticeable response to the onset of the N_2 seeding. Significantly bigger was the difference between discharges #33028 and #33032, during which a notable nitrogen wall inventory had built up. Unlike the gas puff, which was localized in the divertor, the nitrogen inventory is distributed along the main chamber as well[5] and could therefore have a bigger impact on the midplane measurements. The biggest difference between the non-seeded and seeded discharged, however, was observed in the outgassing phase after the end of the discharge. The very noticeable rise of the N_2 pressure is attributed to the release of the plasma-confined nitrogen after the collapse of the pressure gradient. The behaviour of the N_2 signals in the RGAs suggests that the majority of the injected N_2 remains in the divertor, and that a rather small fraction of it enters the plasma from where it is transported (also) to the midplane.
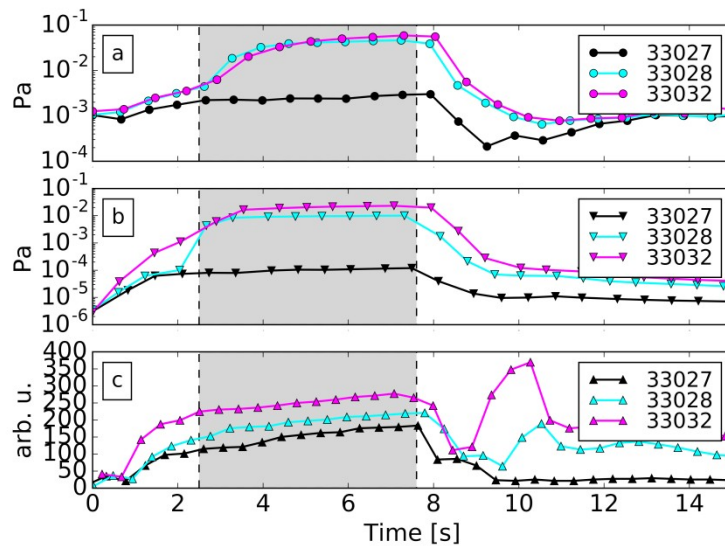

Figure 3:   Partial pressures of N_2 in the inner (a) and outer (b) divertor, and in the midplane, for a non-seeded (33027), the first (33028) and the fifth and N_2-seeded (33032) discharge in the

c. Ammonia

As has been previously reported [4,7,9,10], the mass spectra of ammonia are expected to overlap with those of methane and water, which are also present in the neutral phase during the discharge phases, with varying ratios of hydrogen and deuterium atoms. In order to distinguish between the contributions of the three impurities to the mass spectrometer recordings, a statistical model, described in detail in [7,10] has been fit to the data. In short, the model assumes that each impurity can appear in any of its hydrogen isotope configurations, with a probability determined by the average hydrogen isotope ratio of the impurity.

The time traces of the identified partial pressures of water, methane and ammonia with the RGAs are shown in Fig. 4, for the reference non-seeded discharge #33027 and N₂-seeded discharge #33032. A 10 % uncertainty in the cracking patterns was assumed in the fit. To improve the accuracy of the fit, the isotope ratio of the methane in the model was limited to 5 % hydrogen, as it has been shown that the isotope ratio of methane is very close to that of the plasma fuel [11]. The isotope ratio of the water molecules was determined in the non-seeded discharge. In the inner (a) and the outer (b) divertor, the water content in the non-seeded discharge was similar, however, the water in the inner divertor was found to be purely protonated whereas in the outer divertor, the isotope ratio was found to be between 10 % and 15 %. In both locations, the methane was found to be almost exclusively deuterated. The pressure of methane in the inner divertor was between $1 \cdot 10^{-2}$ Pa and $1 \cdot 10^{-2}$ Pa, and around $1 \cdot 10^{-4}$ Pa in the outer divertor. This difference in the pressures was consistent with the cryo panel induced pressure drop measured in D₂. In contrast, the water pressure in both clusters was around $1 \cdot 10^{-3}$ Pa.

In the midplane (e), water was the most prominent impurity in the discharge phase as well, with approximately three times higher pressure than methane. Unlike in the divertor, a slight increase in the pressures was observed after the discharge phase. In all three locations, for the non-seeded discharges, the fit reported non-zero pressures of ammonia. As no ammonia formation was expected in a non-seeded discharge[4,7,12,13], the reported ammonia pressures from the non-seeded discharge can serve as an estimate of the reliability of the detection.

Both in the inner (b) and outer (d) divertor, ammonia was clearly detectable in the discharge phase of the seeded discharge. The highest pressure of ammonia was observed in the inner divertor, where it corresponded to a 2 % concentration in the neutral gas, and was an order of magnitude higher than the impurity partial pressures in a non-seeded discharge. The pressure began to rise approximately a second after the onset of N₂ seeding, continued to increase linearly throughout the discharge and then decreased rapidly after the end of the discharge phase. Similar trends were observed in the outer divertor, however there, the pressure of ammonia was two orders of magnitude lower, and water remained the most prominent impurity. Although this reduction in pressure is far greater than that observed in D₂ or methane, it could still be in a great part attributed to the cryo panel. Unlike D₂, methane and N₂, ammonia is likely pumped by the liquid N₂ shield which has a larger surface area than

the cryo panel and therefore a higher pumping speed. Additionally, ammonia could also be pumped by the surfaces of the pump duct leading to the RGA, due to its high sticking probability[14], which is discussed later in this section. It is also noteworthy that the pressure of methane decreased (in both divertor legs) with the onset of N_2 seeding, indicating a reduction of the erosion of carbon from the plasma-facing surfaces. In the midplane, a faint signal of ammonia was detected only in the outgassing phase. As described in [10], the uncertainty in the detection of individual species stems from the sensitivity of the fitting procedure to the uncertainty in the used cracking patterns. Thus, the amounts of ammonia reported in the midplane RGA recordings are around the noise level.

The observed distribution of the detected ammonia is in line with previous reports[12,13] which predict that ammonia is formed in surface reactions between nitrogen and hydrogen (or, in this case, deuterium) atoms, and that the ammonia molecules which re-enter the plasma phase are dissociated with a very high probability[15,16]. As the flow of nitrogen atoms from the plasma in the midplane was not significantly increased compared to non-seeded discharges, no formation of ammonia was observed there in the discharge phase. At the same time, the ammonia formed in the divertor could not migrate to the midplane in the discharge phase as it was promptly dissociated to N and D atoms in the plasma. Thus, no ammonia could be detected in the midplane before the end of the discharge.

In the inner divertor, the trend of the identified partial pressure of water followed that of ammonia, which could indicate that water is being substituted for ammonia in the fitting procedure. To account for this uncertainty, two versions of the model were fitted to the data: with and without water as a candidate species, and the resulting identified ammonia pressure were the mean values of the two fits. However, the uncertainty of the ammonia detection in the divertor was relatively low. In the inner divertor, the partial pressure of ammonia exceed that of water by an order of magnitude, so any substitution of water would make a relatively small contribution to the signal. In the outer divertor, the ammonia was easier to separate from water due to the bigger difference in their hydrogen isotope ratios.
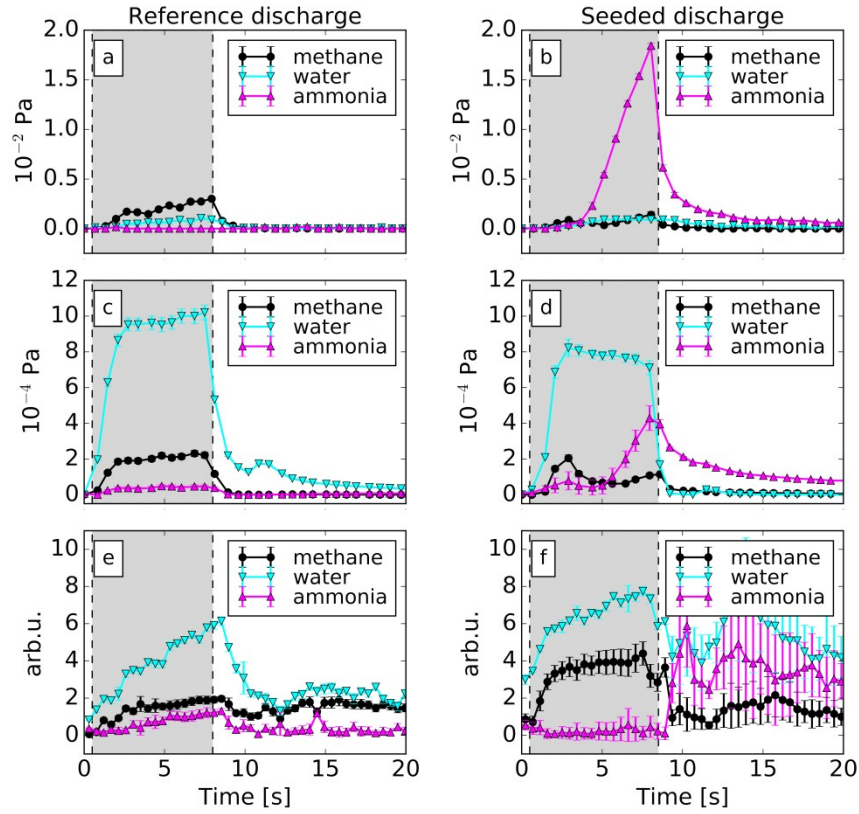
Figure 4: Identified partial pressures of water, methane and ammonia by RGA in the inner divertor (a, b), outer divertor (c, d) and in the midplane (e, f), in a non-seeded (a, c, e) and N $_2$-seeded (b, d, f) discharge. The grey strips indicate the discharge phase.

Previous reports from AUG[7] and JET[4], as well as laboratory experiments[14] indicate that the detection of ammonia could be affected by the sticking of ammonia to surfaces between the region of formation and the location of the mass spectrometer. The sticking of ammonia is considered for the mass spectrometer in the inner divertor, which is located in a differentially pumped chamber, connected to the port of the vacuum vessel of AUG with a 1.5 m long bellow tube. The sticking of ammonia is considered in a zero-dimensional model, where the flow rate of ammonia, Q, into the orifice of the bellows is assumed to have the same trend as the intensity of the emission of the ND radical observed in the divertor spectroscopy (see next section).

The pressure of ammonia, p, in the differentially pumped chamber, represented by the bellows tube, is then determined with the following set of differential equations:

$$\frac{dp}{dt} = \frac{Q(t)}{V} - \frac{S}{V} - \mu \frac{A}{V} e^{-\vartheta(t)} + \frac{1}{\tau} kT\sigma \frac{A}{V} \vartheta(t)$$

$$\frac{d\vartheta(t)}{dt} = \frac{1}{4}\dot{v}\frac{p(t)}{kT}e^{-\vartheta(t)} - \frac{\vartheta(t)}{\tau}$$

where V and A are the combined volume and surface area of the bellows tube ($1.9 \cdot 10^{-3}$ m^3 and 0.64 m^2 respectively), S is the pumping speed of the pump (84 l/s), μ is the sticking coefficient of the ammonia to the bellows surface, ϑ is the degree of saturation of the surface with ammonia, τ the characteristic desorption time of the ammonia molecules from the bellows surface, k the Boltzmann constant, T the temperature of the gas and σ the saturated surface density of ammonia. The pumping speed was estimated from the ratio of pressures measured outside and inside the bellows. The solution, shown in Fig 5, was evaluated for the trends measured in discharge #33038. In this discharge, the N$_2$ seeding lasted only until the 5.5 s mark, and was followed with a 2 s long non-seeded phase. This discharge provided the biggest variation of the ammonia trends within the discharge phase, in which we expected the transport of gas towards the RGA to be unchanged, and the observed trends in the RGA signal was not affected by the change of the transport at the end of the discharge after 8 s, as seen in Fig. 3.
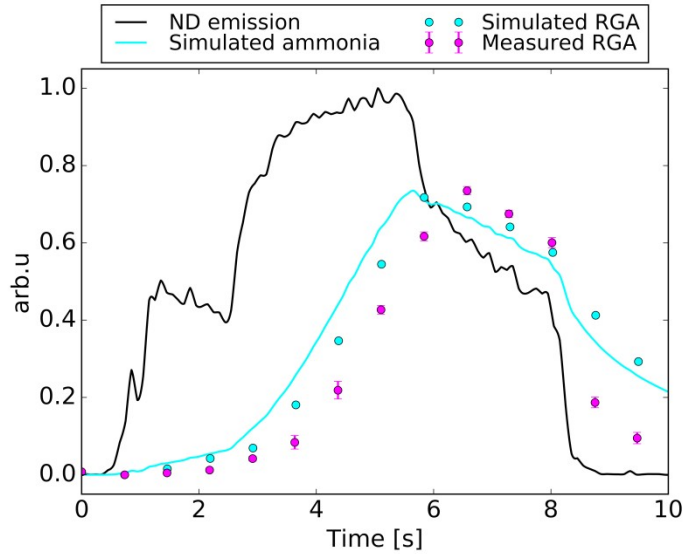

Figure 5:   Simulated and recorded pressure of ammonia in the differentially pumped chamber of the inner divertor mass spectrometer in discharge #33038. The ND emission trend represents the flow of ammonia into the chamber. The simulated pressure of ammonia is additionally delayed by taking into account the limited time resolution of the mass spectrometer.

De Castro et al[14] report a sticking coefficient of 0.08 at room temperature, and very high surface inventory of ammonia, however their experiments were conducted with pure ammonia, on a well-defined stainless steel surface. In the presented experiment, the gas mixture was dominated by D$_2$, followed by N$_2$ at roughly 10 %. The concentration of ammonia was of the order of 1 %, and the state of the surface was unknown. It is reasonable to expect that, over several years of AUG operations (including with the carbon wall configurations), the inner surface of the bellows tube had become contaminated with various deposits.

Due to the unknown surface conditions, the validity of the model was then limited to the qualitative interpretation of the observed trends of the ammonia pressure. The aim of the fitting was to replicate the two main characteristics of the RGA signal: the delayed rise with respect to the ND emission at the beginning of the discharge, and the decline after the end of the N_2-seeded phase. The values reported by De Castro et al[14] were used as the initial estimate in the fitting, however both of the aforementioned characteristics could be replicated with values of μ ranging from 0.05 to 1.0. However, in each case, the saturation surface density of ammonia was found to be significantly smaller than in [14]. The model did not take into account the change of the gas transport and pumping properties brought on by the collapse of the pressure gradient at the end of the discharge, which explains the discrepancy between the model and the experimental data after the time of 8 s.

The findings of this calculation are therefore that while the ammonia pressure, detected by the mass spectrometer, generally follows the trend of the ammonia pressure in the divertor, there is noticeable delay and attenuation of the detected pressure due to the sticking to, and subsequent release from the surfaces between the divertor and the mass spectrometer. Therefore, the measurements of the mass spectrometers need to be integrated over the whole duration of the discharge and the outgassing phases, in order to obtain the full information of the detected impurities.

4. Divertor spectroscopy

The divertor spectroscopy was performed with a visible and near UV spectrometer, tuned to the wavelength range from 321 to 342 nm, with the resolution of 0.02 nm. The integration time was set to 5 ms, and the signal was down-sampled to 10 samples per second to reduce the noise. The lines of sight (LOSs) are shown in Fig. 4. For each leg of the divertor, there are four LOSs which look exclusively into the divertor (RIN002, RIN001, RIV006 and RIV004 in the inner divertor, WOC006 – WOC001 in the outer divertor). Additionally, seven more LOSs were used, which look along the high and low field side scrape-off layer (RIN004 and DOT002 respectively), across the divertor just below the X-point (RXV001) and into the core plasma at different distances from the divertor (RTN001, RTN005, RH2-2, RH2-4).
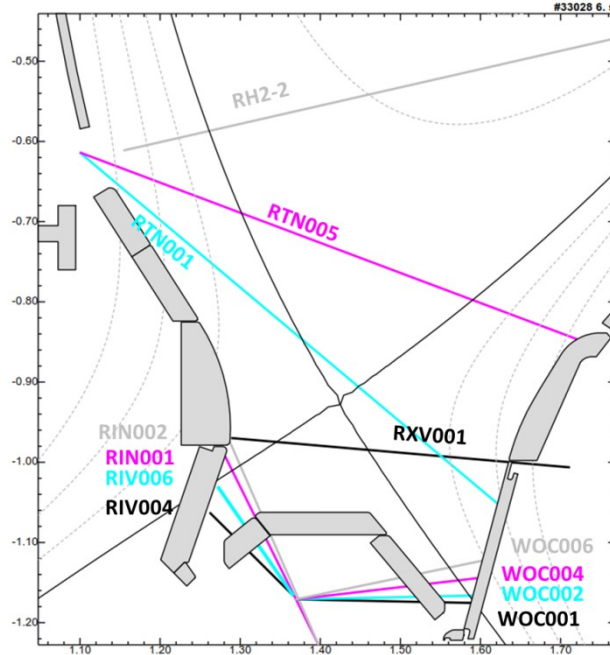
Figure 6:   Divertor spectroscopy lines of sight

In the observed spectral range, the presence of ammonia in the plasma edge is indicated by the emission of the ND spectral system (A$^3\Pi$ – X$^3\Sigma$), as has been shown in laboratory discharges[16] as well as at JET[17]. This radiation is attributed to the ND radical which, in turn, is created by dissociation of ammonia (ND$_3$) molecules.
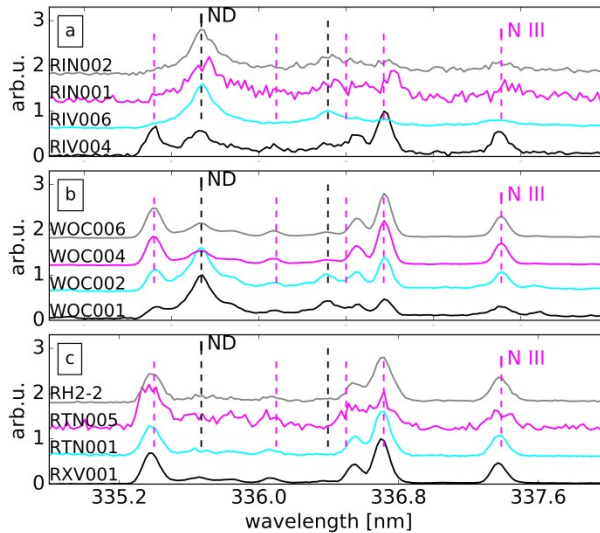

Figure 7:   Normalized spectra in the inner (a) and outer (b) divertor region, and near the x-point (c), from t = 6.8 s in discharge #33032

Fig. 7 shows normalized spectra recorded in the lines of sight crossing each of the divertor legs, and the main plasma volume below and above the X-point. In the shown spectral region, 335 – 337 nm, several N III lines are present beside the ND system. In the main plasma volume the shape of the spectrum did not change significantly – in all LOSs the N III were clearly observable while the ND system was not. The ND system was observed only in LOSs that crossed the legs of the divertor. The highest relative intensity of the ND peaks was observed at the LOSs that were closer to the strike point. In the outer divertor, this was at the lowermost LOS (WOC001). In the inner divertor, the LOS below the strike point (RIV004) showed a significantly lower intensity of the ND radiation. In the inner divertor, the ND radiation was the most prominent spectral feature, clearly dominating over the N III radiation in all lines of sights above the strike point. Below the strike point (RIV004) however, the N III lines were more prominent that the ND system. In the outer divertor, the relative intensity of the N III lines was stronger. The ND system dominated only the lowermost two LOSs and almost vanished in the highest LOS (WOC006).

The observed distribution of the ND radiation is in line with the interpretation that ammonia is formed in surface reactions between atoms impinging from the plasma. Their highest flux density is at the strike point and accordingly, this is where the highest ND emission was observed. The surface-formed ammonia desorbs and is dissociated to N and D atoms in the plasma phase, which explains the diminishing ND emission in the higher LOSs. As no ammonia can therefore penetrate into the main plasma volume, these results are also in line with the distribution of the ammonia in the neutral gas. The weakest N III radiation was observed in the inner divertor which, in contrast to the outer, was fully detached. The lower electron temperature could thus account for a lower degree of ionization of the N atoms, as well as for a lower rate of dissociation of the surface-formed ammonia molecules and explain the slightly greater depth of penetration of the ammonia towards the main plasma volume.

Spectra from the RIV006 LOS (where the ND emission was the most prominent) recorded 1.8 s (reference phase), 6.8 and 7. 5 s (flat-top seeded phase) were fit with a model described in [18], as seen in Fig 8. The identified rotational and vibrational temperatures of the ND radical are listed in Table 2. Throughout the course of the discharge, only minor variations in both temperatures were identified. Because the change of the spectrum did not change considerably with the changes in nitrogen density and other parameters between the reference and the seeded phase, the intensity of the main ND peak at 335.68 nm was used as the measure for the ND emission.
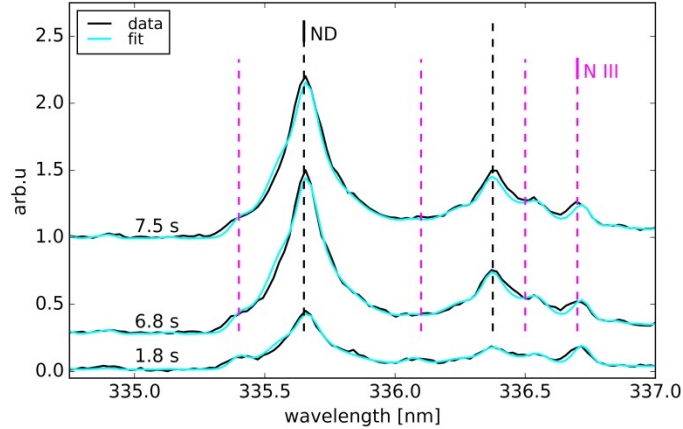
Figure 8:   Spectra from various phases of discharge #33032 seen in the LOS RIV006, and the fitted model. The fitted temperatures are listed in Table 2.

Table 2: Values of the rotational and vibrational temperatures of the ND radical, obtained from fitting the model to spectra recorded in the LOS RIV006 in discharge #33032

Time [s]	T_{rot} [K]	T_{vib} [K]
1.8	5570 ± 170	4550 ± 150
6.8	5700 ± 90	4430 ± 70
7.5	5700 ± 90	4430 ± 70

5. Build-up of nitrogen concentration and ammonia formation

Density of nitrogen in the core the plasma was measured with charge exchange recombination spectroscopy (CXRS)[19], with the outermost line of sight (6.3 cm inboard from the separatrix), and is hereon referred to as the edge density of nitrogen. The time traces of the edge nitrogen density are shown for discharges #33029 through #33032 in Fig 9. The grey bars in the plots indicate time intervals from which data representing the reference and the seeded phase is taken. The mean values of the time traces from those intervals in the range of discharges from #33028 to #33033, is shown in Fig. 10. As stated in Table 1, these discharges feature the same magnetic configuration, heating, fuelling and N_2-seeding rates. In each discharge, a detectable amount of nitrogen was present in the plasma already in the reference phase, with a decaying intensity. It should be noted that the first discharge shown in Fig. 9 was the second seeded discharge in the row. The preceding discharge, #33028, is not shown as the N_2 seeding rate was significantly lower, however it did leave a detectable nitrogen wall inventory. With the onset of N_2 seeding, the intensity increased significantly and continued to increase, at a significantly slower rate, until the end of the flat-top phase of the discharge. The increase of density was noted over the course of discharges, as well, and saturated at discharge #33033, i.e. the 6th discharge in a row, in

which the plasma was shifted upwards by 3 cm. This behaviour is in line with previous report of the evolution of nitrogen density at AUG[5].
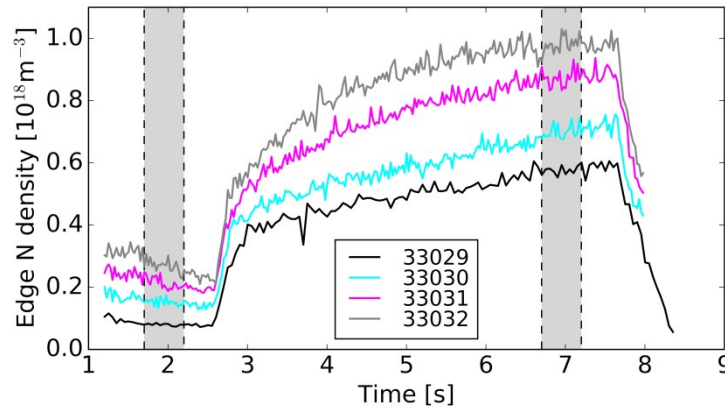

Figure 9:   Time traces of the nitrogen density at the plasma edge from charge exchange recombination spectroscopy. Grey bars indicate the intervals representing the reference and the seeded phases.

Although the absolute values of surface densities of wall-stored nitrogen were contested in later experiments[20–22], the model is still valid in the interpretation that the nitrogen content is strongly contested by the wall condition. The decaying time traces in the reference phase are consistent with a nitrogen plasma content originating from a depleting wall inventory. The density of nitrogen in the seeded phase is consistent with the interpretation that the wall pumping efficiency of nitrogen is reduced as the wall is gradually loaded with nitrogen, which results in higher nitrogen content in the plasma. The influence of the wall inventory indeed had a significant impact on the measured nitrogen density: over the course of four discharges, the nitrogen concentration doubled, at the same N_2 seeding rate, before reaching saturation in the fifth discharge. This then also shows that the N_2 seeding rate alone is not a good parameter of defining the discharge conditions since the nitrogen concentration can vary significantly at a given seeding rate.
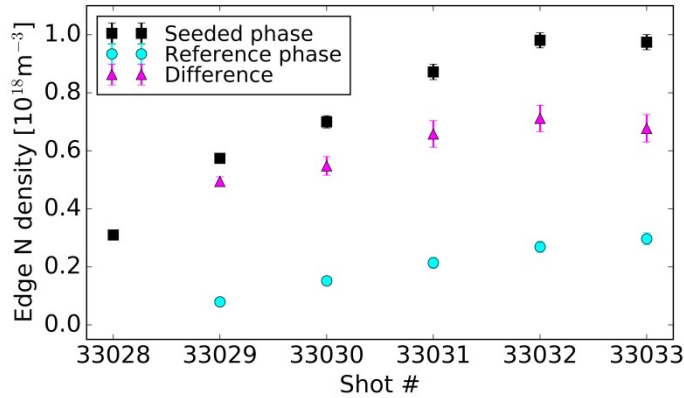
Figure 10: Average values of the edge nitrogen density from CXRS in the reference and the seeded phase of discharges #33028 (shot #1) through #33033 (shot #6), and the difference between them.

Time traces of the ND emission in the inner and outer divertor legs, and the partial pressure of ammonia in the gas pumped from those regions, are shown in Fig 11. The time traces of the ND emission were produced from signals of the LOSs where the ND emission intensity was the strongest, i.e. RIV006 and WOC006. The optical emission spectroscopy time traces exhibited generally very similar trends as observed in the core nitrogen density with CXRS, i.e. gradually decreasing intensities in the reference phase, abrupt jumps with the onset of N_2 seeding, and continuous increase throughout the seeded phase. There are some differences, however. The build-up behaviour within a single discharge was more pronounced in the outer divertor. Moreover, in the inner divertor, the discharge-to-discharge timescale, the ND emission trend saturated at discharge #33032 – one discharge earlier than in the edge nitrogen density.
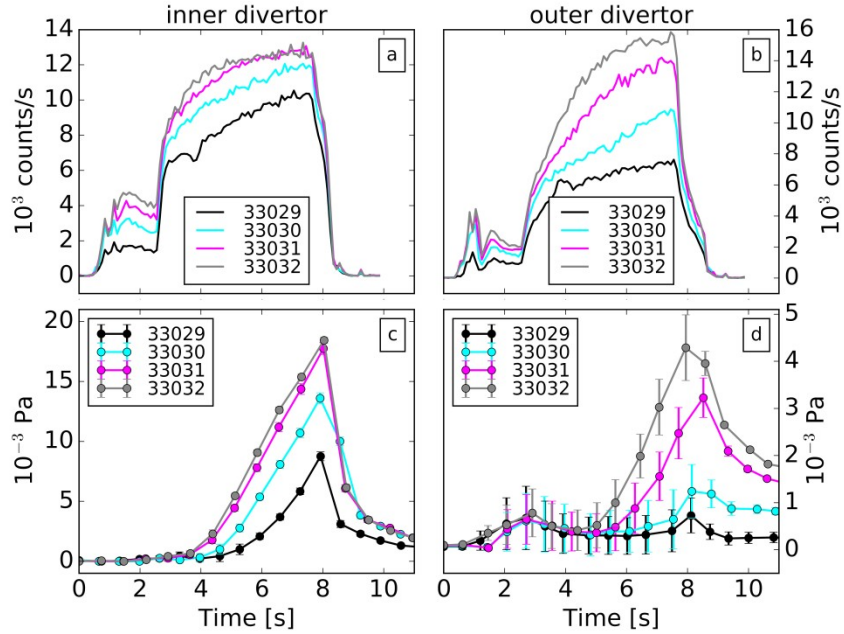
Figure 11:   Time traces of the ND emission (a, b) and partial pressures of ammonia in the neutral gas (c, d) in the inner (a, b) and outer (b, d) divertor, in a series of 4 discharges with the same N_2 seeding rate

Both in the inner and outer divertor, the partial pressure of ammonia in the residual gas and the ND emission showed the same build-up behaviour, which was also similar to that observed in the edge nitrogen concentration. As shown in the previous section, the evolution of the partial pressure, detected by the mass spectrometers, is significantly distorted by the transport of ammonia from the divertor region to the mass spectrometer (i.e. by sticking to surfaces). Combined with the low time resolution of the mass spectrometer (roughly 0.5 s), this makes it impossible to observe the transition from the reference to the seeded phase, and means that the amount of produced ammonia can only be observed by integrating the pressure over the whole duration of the discharge and the outgassing phase. Nevertheless, it is important to note that in the inner divertor, the saturation is observed at the same discharge, which reinforces the interpretation that both the ND emission and that the trends of the ammonia pressure in the residual gas are indeed linked to the ammonia production. Beyond discharge number #33032, the RGA and divertor spectroscopy signals were no longer comparable as the latter were also influenced by the changes in the discharge setup (magnetic configuration in #33033 and reduced power in #33037).

The integral values of the partial pressures of ammonia and nitrogen in the residual gas, are plotted against time-integrated time traces of the core nitrogen density in Fig 12 for all of the performed discharges. Apart from the differences in the absolute values and accuracy already demonstrated and discussed in Fig. 5, the trends of the ammonia content were very similar in all three locations. Namely, the total amount of detected ammonia was proportional to the integrated edge nitrogen density. At a constant flow density of deuterium atoms to the surface, the rate of formation of ammonia in surface

reaction is determined by the flow density of nitrogen atoms [12,13]. While the latter is not directly characterised at AUG, it is reasonable to expect it to be proportional to the density of nitrogen in the divertor plasma which, in turn, at constant discharge conditions is likely proportional to the density of nitrogen at the edge plasma. Thus, the observed behaviour is in agreement with the observed distribution of ammonia which suggests it is formed in surface reactions in the divertor region. The linear trend is somewhat distorted in the midplane (Fig. 12e), however. The outlying data points come from discharges #33037 and #33038 (introduced in the following section). In the latter, the N_2 seeding was stopped 2 seconds before the end of the discharge, allowing enough time for the pressure of ammonia to decay before the outgassing phase and thus making a smaller contribution to the midplane ammonia pressure. In the divertor, the ammonia content in these two discharges did not deviate from the fitted line outside of the usual scatter.

In contrast, the trends of the core nitrogen density are not so well reflected in the detected molecular nitrogen content in the residual gas. In the midplane (Fig. 12.f) and the outer divertor (Fig. 12.d), a straight line could be fitted to the plot, however the intercept of the line was significantly above zero: at a third of the maximum value in the outer divertor and at a half of the maximum value in the midplane. As already noted in Fig. 4, unlike in the divertor, the midplane RGA did not mark as big an increase in the N_2 content in the seeded discharges as the divertor RGAs did. However, even that relatively high background nitrogen content does not fully explain the offset of the trend. In the inner divertor, the trend of the detected N_2 in the discharges with the same amount of injected N_2 (from #33029 onward) was actually reversed. The declining amount of N_2 pressure in the neutral gas is similar to the behaviour of the absolute neutral gas pressure, shown in Figs 13 and 14. Especially in the divertor, the amount of detected N_2 was heavily influenced by the amount of injected N_2, which is demonstrated by the fact that the observed trends were distorted in discharges where a smaller than the standard amount of N_2 was seeded (#33028 and #33038, marked on the plots).
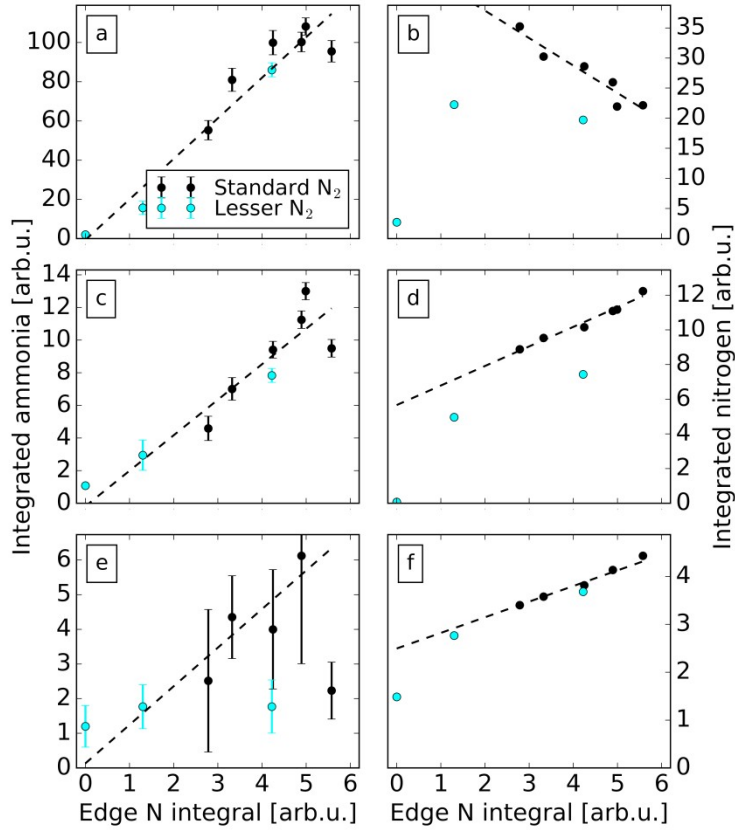
Figure 12: Pulse-integrated partial pressures of ammonia (a, c, e) and nitrogen (b, d, f) in the inner (a, b) and outer (c, d) divertor and the midplane (e, f), shown against pulse-integrated edge nitrogen density from CXRS, from discharges #33027 through #33038

Fig. 13 shows time traces of signals which have been shown to reflect the presence of nitrogen in the plasma [1], in the discharge #33032. The absolute pressure of the neutral gas in the inner and outer divertor is shown in Fig 13a. Both pressure signals increased gradually through the reference phase. At the end of the reference phase, the pressure in the inner divertor was 1 Pa and $4.3 \cdot 10^{-1}$ Pa in the outer divertor. After the onset of nitrogen seeding, the outer divertor pressure increased slightly, to $5.3 \cdot 10^{-1}$ Pa in the first 0.5 s and then still continued to increase with a slower rate, to $6.1 \cdot 10^{-1}$ Pa at the end of the seeded phase. Conversely, the pressure in the inner divertor decreased significantly. The initial decrease started approximately 0.5 s after the start of the N_2 seeding, after which the pressure dropped to $8.3 \cdot 10^{-1}$ Pa in the following 0.5 s. At the end of the seeded phase, it was around $6.9 \cdot 10^{-1}$ Pa. It is noteworthy that despite the increased gas flow, the total neutral gas in the inner divertor did not increase (in contrast to the outer divertor), but in fact started to decrease, which indicates that the behaviour of the gas pressure in the inner divertor is dominated by the collapse of the high-field high density region[23] which has been linked to nitrogen seeding[24].
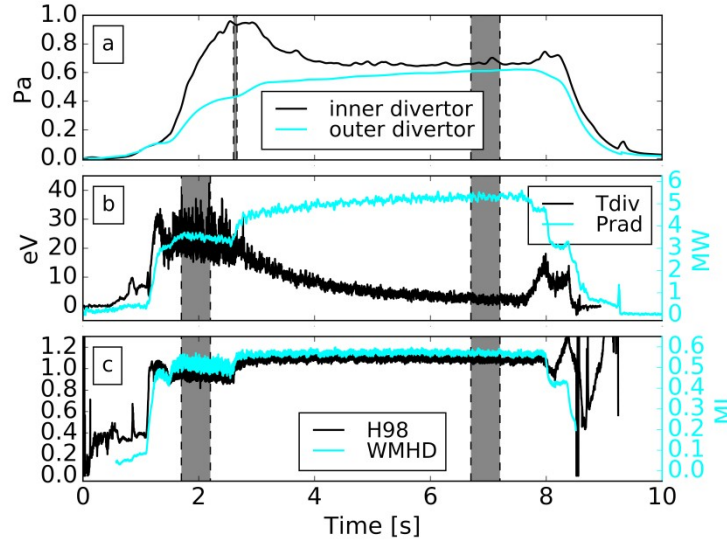
19

Figure 13:   Time traces of absolute pressure in the divertor (a), outer divertor electron temperature and total radiated power (b), and normalized confinement and stored plasma energy (c), from discharge #33032.The grey stripes indicate the reference and seeded phase intervals, relevant for Fig. 10. The absolute pressure values are extrapolated from the direct measurements based on the respective calibration coefficients.

The electron temperature in the outer divertor, determined by shunt current measurements (ref) (Fig. 8b) in the reference phase was around 25 eV. In the seeded phase, it decreased continuously (with no abrupt transition at the start of the seeding) until it stabilized at around 3 eV. The total radiated power (8b) in the reference phase was around 3 MW, in the seeded phase it reached 5.2 MW (60 % of the total heating power) after an abrupt jump and a steady, slower increase. In contrast, the normalized confinement and stored energy (8c) exhibited no significant evolution, except for the abrupt increase at the beginning of the seeded phase. The normalized confinement increased from 0.95 to 1.1, and the stored plasma energy increased from 0.52 MJ to 0.57 MJ. The grey bars in the plots indicate the time intervals from which reference and seeded phase data is extracted (as mean values of all data points within the intervals). Note that to accommodate for the slower build-up of the absolute pressure, the reference phase data are taken from a later interval ($2.60 - 2.66$ s) than for the other signals.

As in the frame of a single discharge, clear evolution was observed in the signals in the whole series of the discharges. The average values of some of the signals are plotted against the average values of the edge nitrogen density from the reference and seeded phases of discharges #33027 through #33033 in Fig. 14. The values of the neutral gas pressure in the inner divertor (a) decreased from 1.1 Pa to 0.9 Pa and down to 0.65 Pa in the reference and seeded phases respectively, the electron temperature decreased (b) from 35 to 20 eV and from 20 to 3 eV, the radiated power (c) rose from 2.3 to 3.6 MW and from 3.9 to 5.2 MW, the normalized confinement from 0.83 to 0.95 and from 1.00 to 1.08, the stored plasma energy (d) from 0.46 to 0.52 MJ and from 0.53 to 0.57 MJ. In both phases, the evolution of all of the signals followed the evolution of the nitrogen edge density, at least up to the density of $0.8 \cdot 10^{18}$ m^{-3}. Moreover, in most cases, the transition between the reference and seeded phase values

was relatively smooth. This would indicate that the source of nitrogen in the plasma (i.e. wall inventory or gas puff) has a significantly smaller effect on the observed signals than the concentration of nitrogen in the plasma.
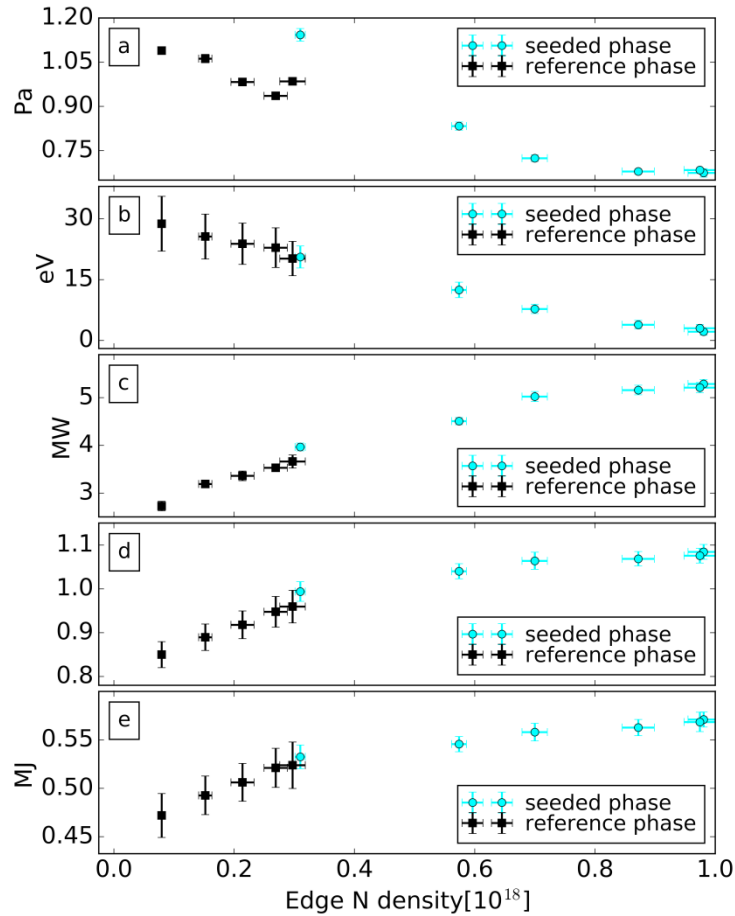

Figure 14:   Average values of the inner divertor neutral gas pressure (a), outer divertor electron temperature (b), total radiated power (c), normalized confinement (d) and stored plasma energy (e) from the reference and seeded phases of discharges #33028 through #33033, as functions of the core nitrogen density (from CXRS)

6. Discharge parameter variation

The series of identically setup discharges, ending at discharge #33032, was followed with an upwards shift of the plasma by 3 cm (#33033) and a discharge with reduced heating (see Table 1) which caused full detachment in the outer divertor (#33037). The partial pressures of ammonia in the inner and outer divertor, the outer divertor electron temperature and the core nitrogen densities are shown in Fig. 15, for discharges #33032, #33033 and #33037. In the inner divertor, raising the plasma did not have a

noticeable effect on this parameter variation, whereas a minor increase could be seen in the detached discharge. In contrast, in the outer divertor, the partial pressure of ammonia had not yet reached saturation in discharge #33032, and continued to increase throughout the range of the following discharges (up to #33037), however with smaller increments. A small increase was observed in the nitrogen density in the plasma edge (d) in discharge #33037, which, again, is in line with the model [5] as a lower heating power would allow for a higher nitrogen wall inventory and consequentially, higher nitrogen plasma content.
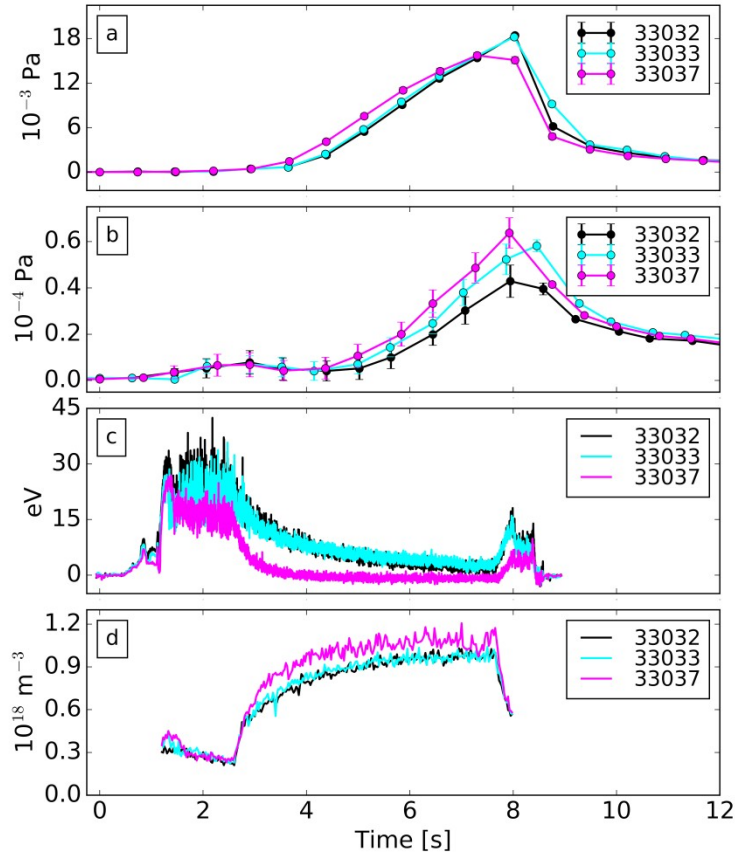

Figure 15: Time traces from discharges #33032, #33033 and #33037. a: partial pressure of ammonia in the inner divertor, b: partial pressure of ammonia in the outer divertor, c: outer divertor electron temperature, d: core nitrogen density from CERS, e: edge nitrogen density from CXRS

The consequences of the full detachment in the outer divertor (Fig. 15 c) were also observable in the spectroscopy signals. The spectra, recorded in the flat top of the seeding phases of discharges #33032 and #33037 are shown in Fig. 16. Compared to the standard setup discharge #33032, the spectra in discharge #33037 had lower overall intensity, which could be related to the decreased heating power. More remarkably, in the fully detached outer divertor, the prominence of the ND system rose compared to the standard discharge. In the LOSs closer to the main plasma volume, the N III lines dominated the spectra in the standard discharges. With a fully detached divertor, however, the relative intensity of the

N III lines decreased more than the relative intensity of the ND system, making thus the latter the most prominent feature in the spectra.
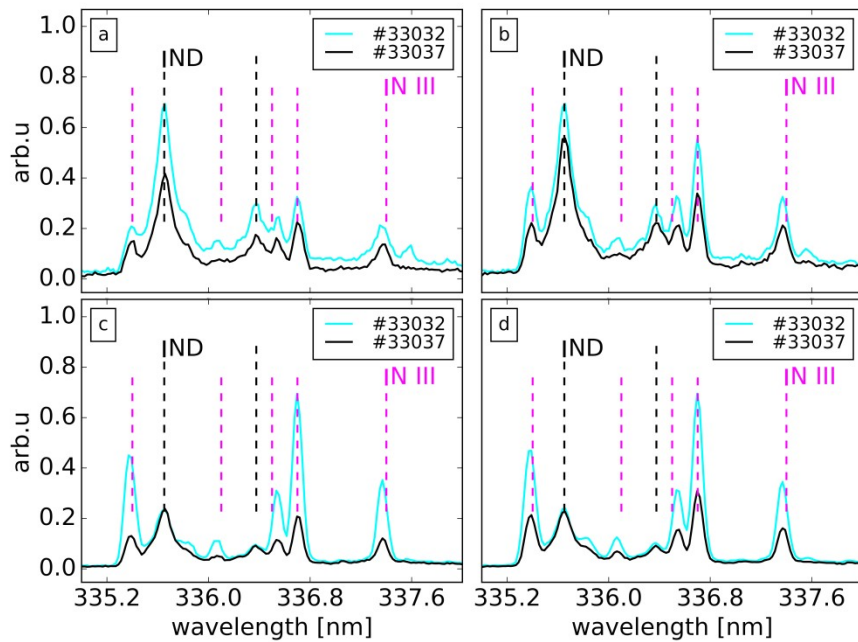

Figure 16: Spectra in the outer divertor, recorded in the flat-top of the seeded phases of discharges 33032 and 33037, in LOSs WOC001 (a), WOC002 (b), WOC004 (c) and WOC006 (d)

Time traces from the last discharge in the row, #33038, are shown in Fig. 17, together with time traces from discharge #33032 for comparison. The setup of this discharge was the same as in discharges #33029 – #33032, except that the nitrogen seeding lasted only until 5.5 s (with the same seeding rate). The seeded phase of #33038 was thus followed by a full-power cleaning phase, lasting from 5.5 s until 7.5 s. In discharge #33038, the nitrogen density in the edge (17a) was considerably higher than in discharge #33032, both in the reference as well as in the seeded phase. In (roughly) the first 0.3 s of the cleaning phase, the density marked an abrupt decline and then continued the same trend as in the reference phase, consistent with depleting the wall nitrogen inventory. The emission of the ND radical in the inner divertor (b) marked a similar decrease and followed the same trend. The increased nitrogen density was reflected in the partial pressure of ammonia in the neutral gas (c), which once again outlines the dependence of the ammonia production on the nitrogen density in the plasma. Moreover, these results show that, at same N_2 seeding rates, a discharge with a lower heating power will leave a detectably higher nitrogen wall inventory.
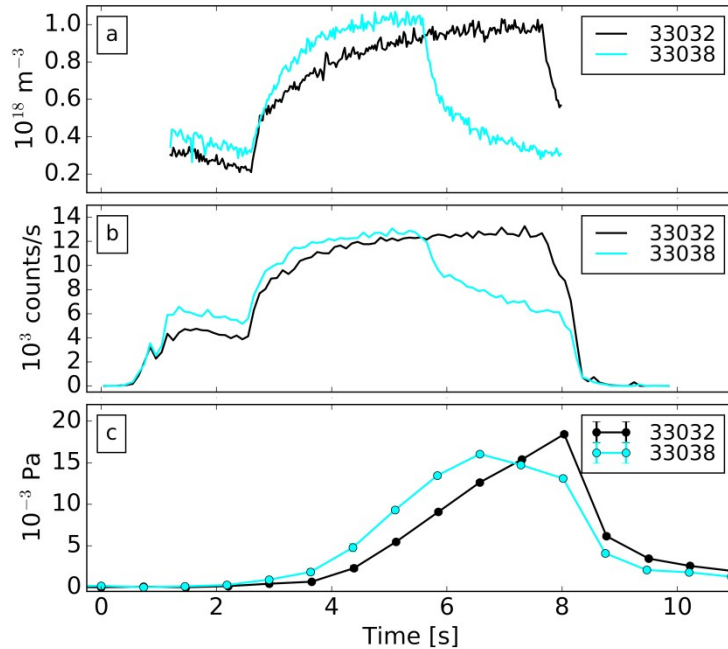
Figure 17: Time traces of the the core nitrogen density from CXRS (a), ND emission intensity in the RIV006 divertor spectroscopy line of sight (b) and partial pressures of ammonia in the inner divertor (c) from discharges #33032 and #33038

7. Conclusions

Ammonia formation was studied in a series of nitrogen seeded H-mode discharges at ASDEX-Upgrade. To aid the study of the evolution of the ammonia formation, all discharges were set-up in the same way, and featured a long, stable flat-top phase. In all discharges, ammonia formation was confirmed with divertor spectroscopy, by observing the emission of the ND radical, and by detectable concentrations of ammonia in the neutral gas. In line with previous observations[7], the signals of ammonia in the neutral gas were significantly delayed compared to the spectroscopy signals, which was explained by pumping of ammonia by, and subsequent release from surfaces of the pipework connecting the divertor and the neutral gas diagnostics. Over a range of discharges, the divertor spectroscopy and neutral gas signals showed very similar trends, both in the inner as well as in the outer divertor, which serves to confirm the validity of both signals as indicators of discharge-produced ammonia.

Laboratory experiments and modelling predict that ammonia is formed in surface reactions[12,13], and that in the plasma, it is being promptly dissociated to N and D atoms. The presented results do not contradict these findings. With divertor spectroscopy, the ND radical was only observed in the lines of sight crossing the both legs of the divertor. The relative intensity of the ND system was typically the strongest at the bottom of the divertor. Closer to the main plasma, it decreased, and completely vanished in the lines of sight crossing the X-point and the main plasma region. In the discharge phase, ammonia was detected only in the neutral gas pumped from the divertor region whereas in the midplane it was detected only in the outgassing phase, following the discharge.

The nitrogen density at the plasma edge, observed with charge exchange spectroscopy, was greatly impacted by the wall inventory: at the same seeding rate, the nitrogen concentration in the plasma could differ by a factor of almost 2, which is in line with previous reports of similar variations[5]. The evolution of the nitrogen concentration was reflected on indirect indicators of the nitrogen content, i.e. radiated power, outer divertor electron temperature, normalized confinement, both in the seeded phase of the discharge when the dominant source of the nitrogen was the N_2 gas puff, as well as in the reference phase when the only source of nitrogen in the plasma was the wall inventory, left over from previous discharges.

The nitrogen plasma content was also found to be the main influence on the ammonia formation. The amount of ammonia, detected in the neutral gas, was proportional to the time-integrated nitrogen density at the plasma edge from charge exchange spectroscopy. Other plasma parameters, albeit explored only in a narrow range, did not have an observable effect on the amount of produced ammonia. This lends credence to the model that ammonia is formed in surface reactions on plasma facing and especially nearby recessed areas. There, the rate of ammonia formation would be mainly defined by the flow density of impinging nitrogen atoms which is expected to be proportional to the nitrogen content in the divertor plasma. In turn, at constant discharge conditions, the divertor nitrogen content is expected to be reflected in the nitrogen density at the plasma edge.

In contrast, the evolution of the nitrogen plasma content was not reflected in the concentration of nitrogen (N_2) in the neutral gas. In the outer divertor and at the midplane, the offset in the linear dependence of the N_2 content suggested that the composition of the neutral gas is dominated by the gas injection, and that likely a significant fraction of the injected N_2 is pumped out without being ionized and entering the main plasma. In the inner divertor, the trends of the detected N_2 suggested that, beside the N_2 gas injection, it was also significantly affected by the neutral gas pressure which in turn is affected by the evolution of the high field side density.

These results highlight the uncertainty regarding the concentration of nitrogen in the divertor plasma. While the nitrogen content in the core plasma is adequately measured with the charge exchange spectroscopy, the nitrogen content in the divertor plasma is still uncharacterised. Moreover, variations in the nitrogen content clearly show that the N_2 seeding rate alone does not sufficiently determine the nitrogen concentration. This uncertainty prevented the assessment of the nitrogen-to-ammonia conversion fraction, despite having quantified the ammonia formation.

Nevertheless, the obtained results provide very direct evidence that the rate of ammonia formation is defined by the nitrogen density in the divertor plasma, which explains the evolution of ammonia formation observed both in this as well as previous experiments. Moreover, they validate residual gas analysis and divertor spectroscopy as means of detection of the discharge-produced ammonia. As the nitrogen content in the plasma, and consequentially the ammonia formation, exhibited a pronounced evolution in each discharge, it would be interesting to perform such experiments in fusion devices capable of very long pulse operation, which would allow to reach the steady state nitrogen concentration and rates of ammonia formation. The observed distribution of the ammonia both in spectroscopy signals as well as in the neutral gas should be considered in preparing future experiments.

At the same time, future efforts should also be focused on determining the true concentration of nitrogen in the divertor plasma.

8. Acknowledgements

9. References

[1]   Beurskens M N A, Dunne M G, Frassinetti L, Bernert M, Cavedon M, Fischer R, Järvinen A, A. Kallenbach, Laggner F M, McDermott R M, Potzel S, Schweinzer J, Tardini G, Viezzer E, Wolfrum E, Team the A U and team the Euro M 2016 The role of carbon and nitrogen on the H-mode confinement in ASDEX Upgrade with a metal wall *Nucl. Fusion* **56** 056014

[2]   Kallenbach A, Bernert M, Dux R, Casali L, Eich T, Giannone L, Herrmann A, McDermott R, Mlynek A, Mueller H W, Reimold F, Schweinzer J, Sertoli M, Tardini G, Treutterer W, Viezzer E, Wenninger R, Wischmeier M and Team A U 2013 Impurity seeding for tokamak power exhaust: from present devices via ITER to DEMO *PLASMA Phys. Control. FUSION* **55**

[3]   Van Hoey O, Kirschner A, Bjrkas C, Borodin D, Matveev D, Uytdenhouwen I and Van Oost G 2013 Improved carbon migration modelling with the ERO code *J. Nucl. Mater.* **438** S891–4

[4]   M Oberkofler and G Meisl and A Hakola and A Drenik and D Alegre and S Brezinsek and R Craven and T Dittmar and T Keenan and S G Romanelli and R Smith and D Douai and A Herrmann and K Krieger and U Kruezi and G Liang and Ch Linsmeier and M Mozetic and V Rohde and the ASDEX Upgrade team and the EUROfusion MST1 Team and JET Contributors 2016 Nitrogen retention mechanisms in tokamaks with beryllium and tungsten plasma-facing surfaces *Phys. Scr.* **2016** 014077

[5]   Kallenbach A, Dux R, Fuchs J C, Fischer R, Geiger B, Giannone L, Herrmann A, Lunt T, Mertens V, McDermott R, R Neu, Pütterich T, Rathgeber S, Rohde V, Schmid K, Schweinzer J, Treutterer W and Team A U 2010 Divertor power load feedback with nitrogen seeding in ASDEX Upgrade *Plasma Phys. Control. Fusion* **52** 055002

[6]   Drenik A, Oberkofler M, Alegre D, Kruezi U, Brezinsek S, Mozetic M, Nunes I, Wischmeier M, Giroud C, Maddison G and Reux C 2015 Mass spectrometry analysis of the impurity content in N2 seeded discharges in JET-ILW *J. Nucl. Mater.* **463** 684–7

[7]   Neuwirth D, Rohde V, Schwarz-Selinger T and Team A U 2012 Formation of ammonia during nitrogen-seeded discharges at ASDEX Upgrade *Plasma Phys. Control. Fusion* **54** 085008

[8]   Carrasco A G, Wauters T, Petersson P, Drenik A, Rubel M, Crombé K, Douai D, Fortuna E, Kogut D, Kreter A, Lyssoivan A, Möller S, Pisarek M and Vervier M 2015 Nitrogen removal from plasma-facing components by ion cyclotron wall conditioning in TEXTOR *J. Nucl. Mater.* **463** 688–92

[9]   PRICE G and IGLESIA E 1989 MATRIX-METHOD FOR CORRECTION OF MASS-SPECTRA IN DEUTERIUM-EXCHANGE APPLICATIONS *Ind. Eng. Chem. Res.* **28** 839–44

[10]   Drenik A, Alegre D, Brezinsek S, de Castro A, Kruezi U, Meisl G, Mozetic M, Oberkofler M, Panjan M, Primc G, Resnik M, Rohde V, Seibt M, Tabares F L, Zaplotnik R, team A-U, team Euro M and contributors J E T 2017 Detection of ammonia by residual gas analysis in AUG and JET *FUSION Eng. Des.* **124** 239–43

[11]   Drenik A, Alegre D, Brezinsek S, De Castro A, Kruezi U, Oberkofler M, Panjan M, Primc G, Reichbauer T, Resnik M, Rohde V, Seibt M, Schneider P A, Wauters T, Zaplotnik R, Team A-U, Team Euro M and Contributors J E T 2017 Evaluation of the plasma hydrogen isotope content by residual gas analysis at JET and AUG *Phys. Scr.* **T170**

[12]   van den Oever P J, van Hemmen J L, van Helden J H, Schram D C, Engeln R, van de Sanden M C M and Kessels W M M 2006 Downstream ion and radical densities in an Ar-NH3 plasma generated by the expanding thermal plasma technique *PLASMA SOURCES Sci. Technol.* **15** 546–55

[13]   Gordiets B, Ferreira C, Pinheiro M and Ricard A 1998 Self-consistent kinetic model of low-pressure N-2-H-2 flowing discharges: II. Surface processes and densities of N, H, NH3 species *PLASMA SOURCES Sci. Technol.* **7** 379–88

[14]   de Castro A, Alegre D and Tabares F L 2016 Physisorption of ammonia on AISI 304 L stainless steel at different surface temperature under high vacuum conditions *Nucl. Mater. ENERGY* **9** 1–5

[15]   Gordiets B, Ferreira C, Pinheiro M and Ricard A 1998 Self-consistent kinetic model of low-pressure N-2-H-2 flowing discharges: I. Volume processes *PLASMA SOURCES Sci. Technol.* **7** 363–78

[16]   Drenik A, Mourkas A, Zaplotnik R, Primc G, Mozetič M, Panjan P, Alegre D and Tabarés F L 2016 Erosion of a-C:H in the afterglow of ammonia plasma *J. Nucl. Mater.* **475** 237–42

[17]   Oberkofler M, Douai D, Brezinsek S, Coenen J W, Dittmar T, Drenik A, Romanelli S G, Joffrin E, McCormick K, Brix M, Calabro G, Clever M, Giroud C, Kruezi U, Lawson K, Linsmeier C, Rojo A M, Meigs A, Marsen S, Neu R, Reinelt M, Sieglin B, Sips G, Stamp M and Tabares F L 2013 First nitrogen-seeding experiments in JET with the ITER-like Wall *J. Nucl. Mater.* **438** S258–61

[18]   Pawelec E, Dittmar T, Drenik A, Meigs A and contributors J E T 2018 Molecular ND Band Spectroscopy in the Divertor Region of Nitrogen Seeded JET Discharges *J. Phys. Conf. Ser.* **959** 012009

[19]   Viezzer E, Puetterich T, Dux R, McDermott R M and Team A U 2012 High-resolution charge exchange measurements at ASDEX Upgrade *Rev. Sci. Instrum.* **83**

[20]   Meisl G, Schmid K, Encke O, Hoeschen T, Gao L and Linsmeier C 2014 Implantation and erosion of nitrogen in tungsten *NEW J. Phys.* **16**

[21]   Meisl G, Schmid K, Oberkofler M, Krieger K, Lisgo S W, Aho-Mantila L, Reimold F and Team A U 2015 Nitrogen retention in ASDEX Upgrade *J. Nucl. Mater.* **463** 668–71

[22]   Meisl G, Schmid K, Oberkofler M, Krieger K, Lisgo S W, Aho-Mantila L, Reimold F, Lunt T and Team A U 2016 Experimental analysis and WallDYN simulations of the global nitrogen migration in ASDEX Upgrade L-mode discharges *Nucl. FUSION* **56**

[23]   Potzel S, Wischmeier M, Bernert M, Dux R, Reimold F, Scarabosio A, Brezinsek S, Clever M, Huber A, Meigs A, Stamp M, Team A U and Contributors J-E 2015 Formation of the high density front in the inner far SOL at ASDEX Upgrade and JET *J. Nucl. Mater.* **463** 541–5

[24]   Reimold F, Wischmeier M, Bernert M, Potzel S, Kallenbach A, Mueller H W, Sieglin B, Stroth U and Team A U 2015 Divertor studies in nitrogen induced completely detached H-modes in full tungsten ASDEX Upgrade *Nucl. FUSION* **55**